**Supplementary file**

# Hotspots for warm and dry summers in eastern Europe, with a focus on Romania

Viorica Nagavciuc[1,2], Patrick Scholz[1] and Monica Ionita[1,3*]

[1]Alfred Wegener Institute Helmholtz Center for Polar and Marine Research, Paleoclimate Dynamics Group, Bremerhaven, Germany
[2]Faculty of Forestry, Ștefan cel Mare University, Suceava, Romania
[3]Emil Racovita Institute of Speleology, Romanian Academy, Cluj-Napoca, Romania

## 1. Ranking maps

In order to analyze the extremeness of the July 2012, August 2015 and Jun 2019 heatwaves, we have made use of the ranking maps methodology (Bakke et al., 2020; Ionita et al., 2017). First, TX90 was computed for the 70-year period (1951–2020), and for each month the years were ordered from the most extreme (highest temperature) to the least extreme value. Then, ranking maps for each event were made by finding the position (rank) of that event if it were among the eight highest TX90 values. A rank of 1 implies record-breaking high temperature (in the case of TX90 ), a rank of 2 indicates that the respective month had the second most extreme value, etc.

## 2. Composite maps

To identify the physical mechanism responsible for occurrence of heatwaves, at country level, we constructed composite maps of the years when the HWDI, at country level, was > 5 days. This threshold was chosen as a compromise between the strength of the climate anomalies associated with monthly HW conditions and the number of maps satisfying this criterion. Further analysis has shown that the results are not sensitive to the exact threshold value used for our composite analysis (not shown). We have computed composite maps, instead of correlation maps, because the former considers the nonlinearities included in the analyzed data. The significance of the composite maps is based on a standard *t-test* (confidence level 95 %).

## 3. 2-D Atmospheric blocking index

The two-dimensional (2D) atmospheric blocking index, used in this study, is based on the definition from (Scherrer et al., 2006). To compute the 2-D blocking index, we have used the daily geopotential height at 500mb extracted from the ERA5 reanalysis project (Hersbach et al., 2020), which has a spatial resolution of 0.25∘ × 0.25∘ and covers the period 1950– 2020. The 2-D blocking index is an extension of the one-dimensional (1-D) Tibaldi-Molteni (TM) index (Tibaldi and Molteni, 1990) to a two-dimensional map of blocking frequencies at every grid point. The southern geopotential height gradient (GHGS) and the northern geopotential height gradient (GHGN) for each grid point are evaluated as follows:

$$GHGS = (Z(\phi_0) - Z(\phi_0 - 15^0))/15^0 \tag{1}$$
$$GHGN = (Z(\phi_0 + 15^0) - Z(\phi_0))/15^0 \tag{2}$$

where $\phi_0$ is the latitude of the considered grid point varying from 35°N to 75°. For each month we have calculated the ratio between the number of days when a certain grid point was blocked, i.e. the conditions GHGS > 0 and GHGN < (-10m/°.lat) are simultaneously satisfied for at least five consecutive days.

## References

Bakke, S. J., Ionita, M. and Tallaksen, L. M.: The 2018 northern European hydrological drought and its drivers in a historical perspective, Hydrol. Earth Syst. Sci., 24(11), 5621–5653, doi:10.5194/hess-24-5621-2020, 2020.

Ionita, M., Tallaksen, L. M., Kingston, D. G., Stagge, J. H., Laaha, G., Van Lanen, H. A. J., Scholz, P., Chelcea, S. M., Haslinger, K., Lanen, H. A. J. Van, Chelcea, S. M., Haslinger, K., Scholz, P., Chelcea, S. M. and Haslinger, K.: The European 2015 drought from a climatological perspective, Hydrol. Earth Syst. Sci., 21, 1397–1419, doi:doi:10.5194/hess-21-1397-2017, 2017.

Scherrer, S. C., Croci-Maspoli, M., Schwierz, C. and Appenzeller, C.: Two-dimensional indices of atmospheric blocking and their statistical relationship with winter climate patterns in the Euro-Atlantic region, Int. J. Climatol., 26(2), 233–249, doi:10.1002/joc.1250, 2006.

Tibaldi, S. and Molteni, F.: On the operational predictability of blocking, Tellus, 42(A), 343–365, 1990.

**Table S1**. Results of the trend analysis for HWDI (Figure 2 – left column). The trend analysis was conducted based on nonparametric Mann-Kendall test. For the E-OBS data set the analysis was performed over the period 1951 – 2020, while for the ROCADA data the trend analysis was performed over the period 1961 – 2013.

| | | HWDI Trend | P-value |
|---|---|---|---|
| June | E-OBS | 0.52 days/decade | 3.37E-5* |
| | ROCADA | 0.66 days/decade | 1.38E-5* |
| July | E-OBS | 0.31 days/decade | 0.0014* |
| | ROCADA | 0.51 days/decade | 0.0027* |
| August | E-OBS | 0.43 days/decade | 0.0022* |
| | ROCADA | 0.60 days/decade | 0.0032* |
| JJA | E-OBS | 1.2 days/decade | 5.23E-4* |
| | ROCADA | 2.0 days/decade | 6.54E-4* |

The null hypothesis of no trend is rejected if the p-values is lower than 0.05 (significance level of $\alpha$ =0.05).
* indicates a statistically significant trend.

**Table S2**. Results of the trend analysis for SPI (Figure5 – left column). The trend analysis was conducted based on nonparametric Mann-Kendall test. For the E-OBS data set the analysis was performed over the period 1951 – 2020, while for the ROCADA data the trend analysis was performed over the period 1961 – 2013.

| | | SPI Trend | P-value |
|---|---|---|---|
| June SPI1 | E-OBS | 0.02 z-scores/decade | 0.576 |
| | ROCADA | -0.02 z-scores/decade | 0.703 |
| July SPI1 | E-OBS | 0.04 z-scores/decade | 0.259 |
| | ROCADA | -0.03 z-scores/decade | 0.655 |
| August SPI | E-OBS | -0.03 z-scores/decade | 0.484 |
| | ROCADA | -0.03 z-scores/decade | 0.656 |
| August SPI3 | E-OBS | 0.04 z-scores/decade | 0.366 |
| | ROCADA | -0.01 z-scores/decade | 0.753 |

The null hypothesis of no trend is rejected if the p-values is lower than 0.05 (significance level of $\alpha$ =0.05).
* indicates a statistically significant trend.

**Table S3**. Results of the trend analysis for the monthly Z500 indices (Figure 13 – right column). The trend analysis was conducted based on nonparametric Mann-Kendall test, for two distinct period: 1950 – 2020 and 1990 - 2020.

| | | Z500 Index Trend | P-value |
|---|---|---|---|
| June | 1950 – 2020 | 2.8m/decade | 0.06 |
| | 1990 – 2020 | 12.5m/decade | 0.005* |
| July | 1950 – 2020 | 2.8m/decade | 0.009* |
| | 1990 – 2020 | 7.5m/decade | 0.001* |
| August | 1950 – 2020 | 4.3m/decade | 0.0007* |
| | 1990 – 2020 | 11.5m/decade | 0.006* |

The null hypothesis of no trend is rejected if the p-values is lower than 0.05 (significance level of $\alpha$ =0.05).
* indicates a statistically significant trend.
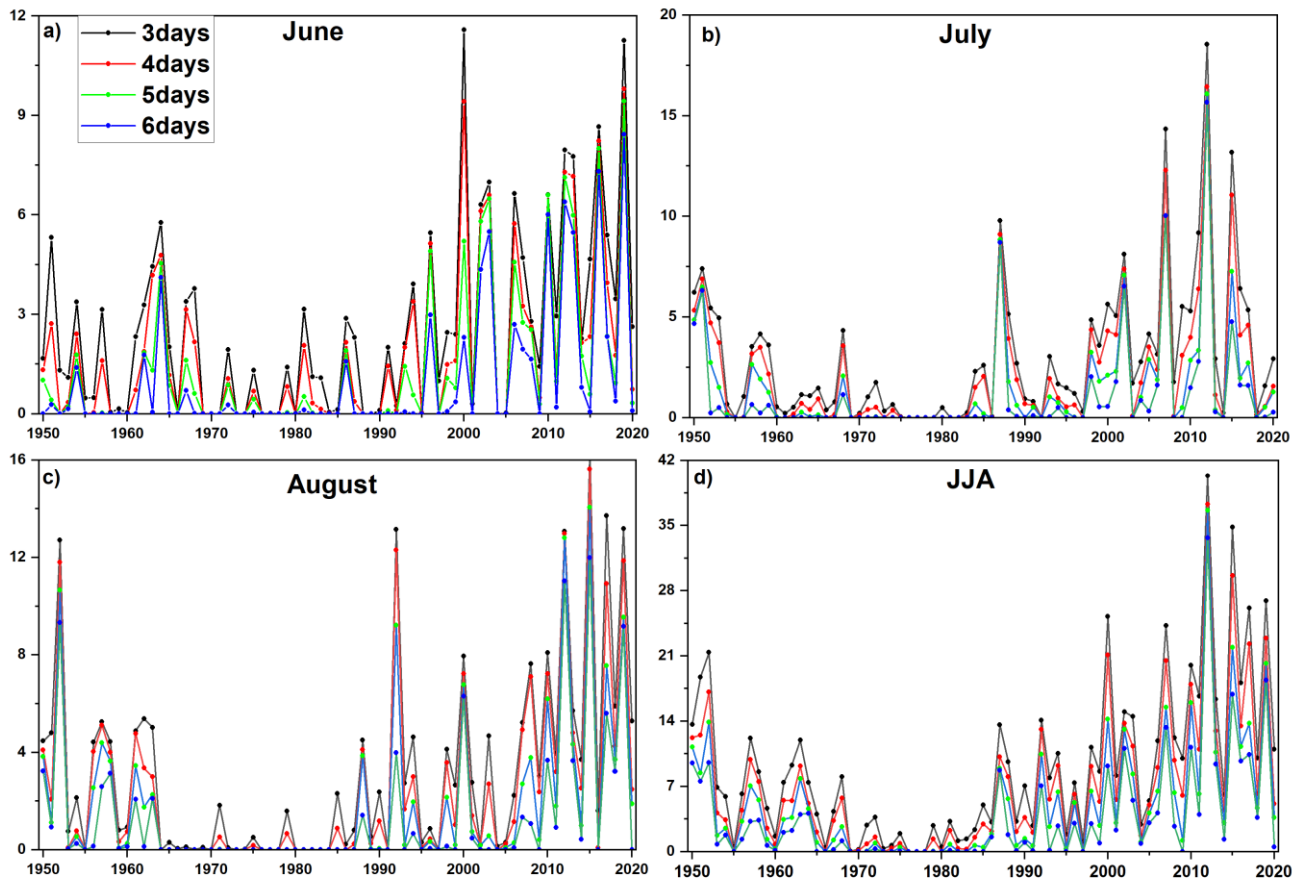
***Figure S1.*** Temporal evolution of the heat wave duration index (HWDI) averaged at country level for different duration: 3 days (black lines); 4 days (red lines), 5 days (green lines) and 6 days (blue lines). a) June; b) July; c) August and d) JJA. Units: a) – c) days/month and d) days/season.
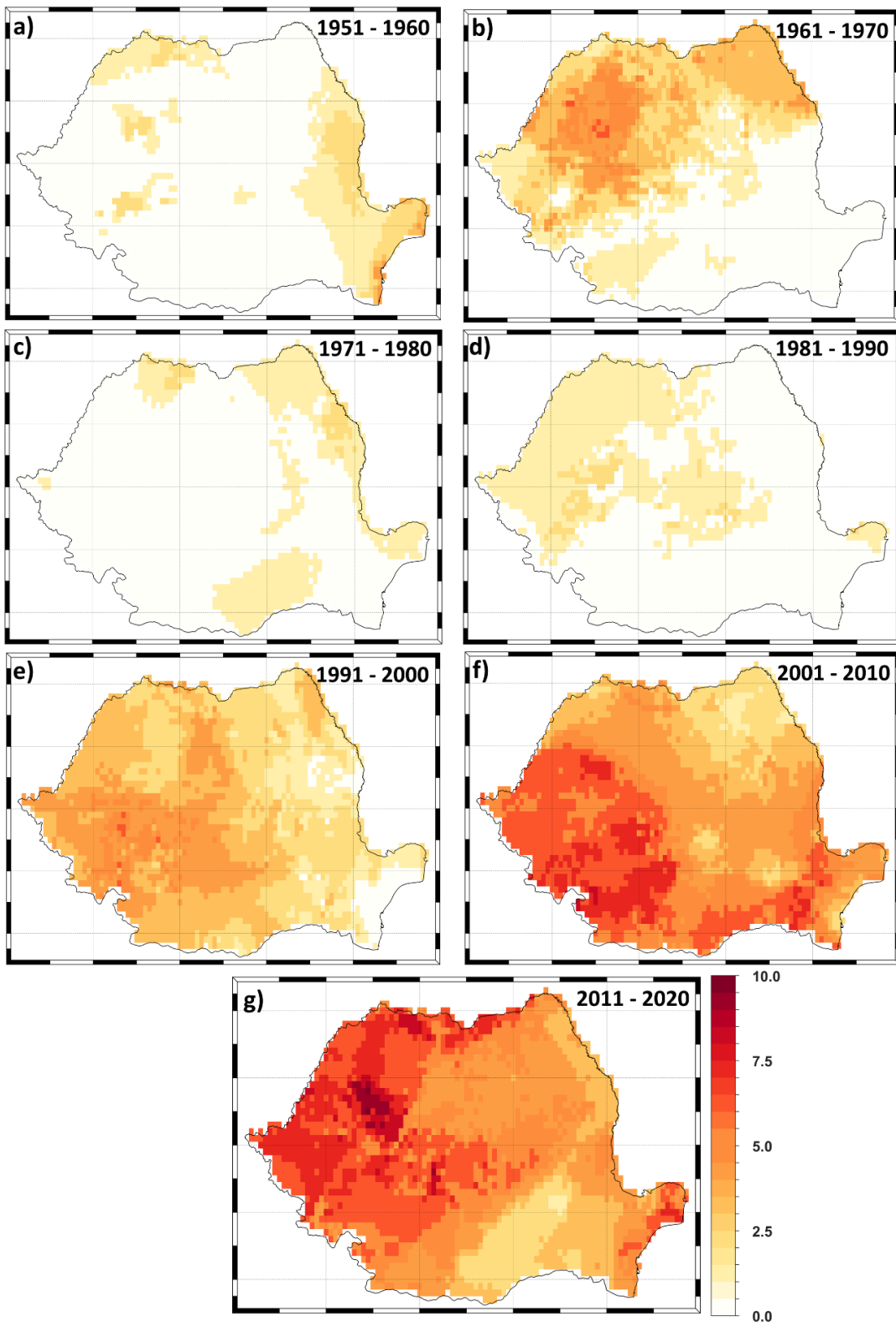
***Figure S2.*** June decadal frequency of the number of heat waves (HWs) per decade over the last 70 years: a) 1951 – 1960; b) 1961 – 1970; c) 1971 – 1980; d) 1981 – 1990; e) 1991 – 2000; f) 2001 – 2010 and g) 2011 – 2020. Units: number of HWs/decade.
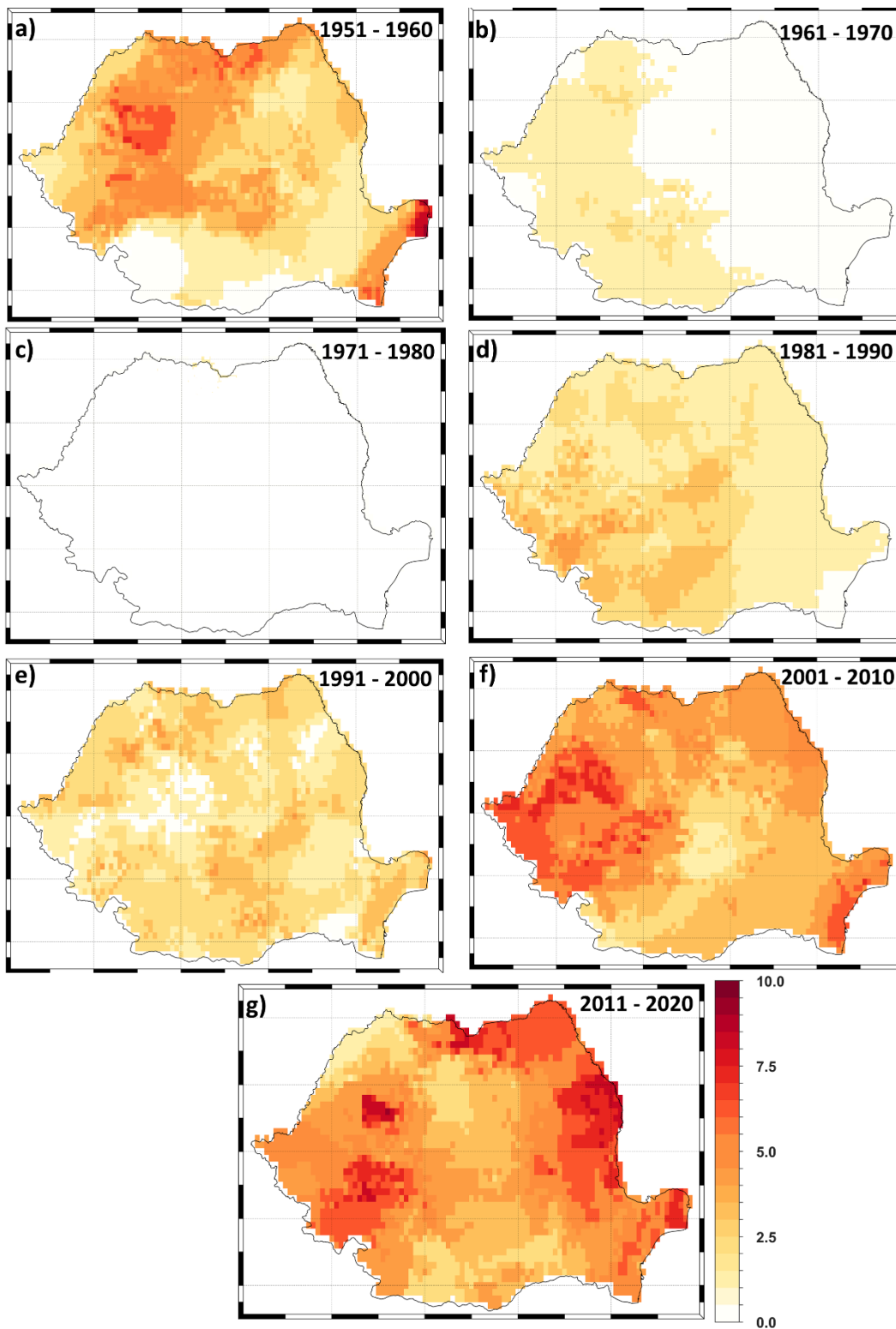
***Figure S3.*** July decadal frequency of the number of heat waves (HWs) per decade over the last 70 years: a) 1951 – 1960; b) 1961 – 1970; c) 1971 – 1980; d) 1981 – 1990; e) 1991 – 2000; f) 2001 – 2010 and g) 2011 – 2020. Units: number of HWs/decade.
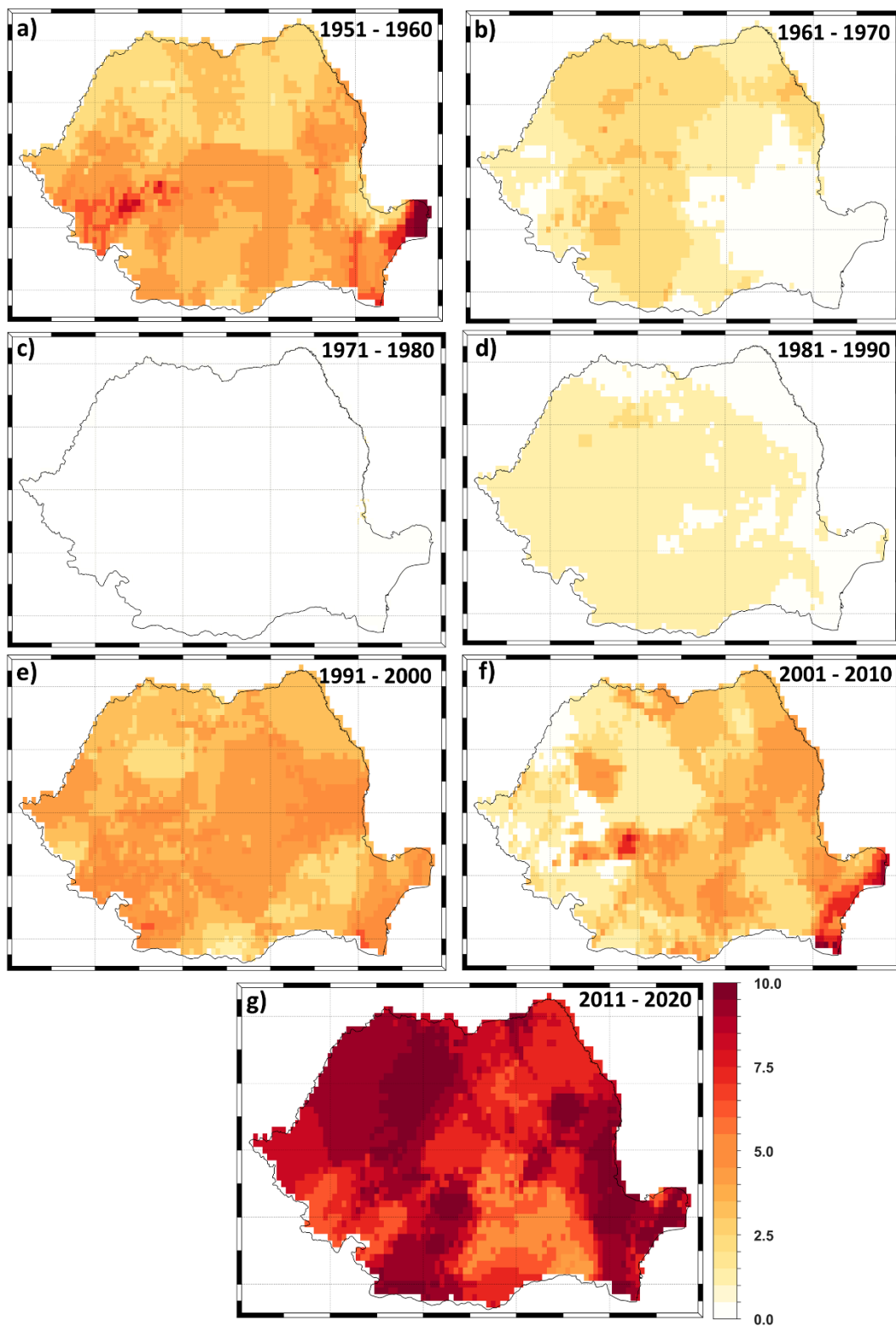
**Figure S4.** August decadal frequency of the number of heat waves (HWs) per decade over the last 70 years: a) 1951 – 1960; b) 1961 – 1970; c) 1971 – 1980; d) 1981 – 1990; e) 1991 – 2000; f) 2001 – 2010 and g) 2011 – 2020. Units: number of HWs/decade.
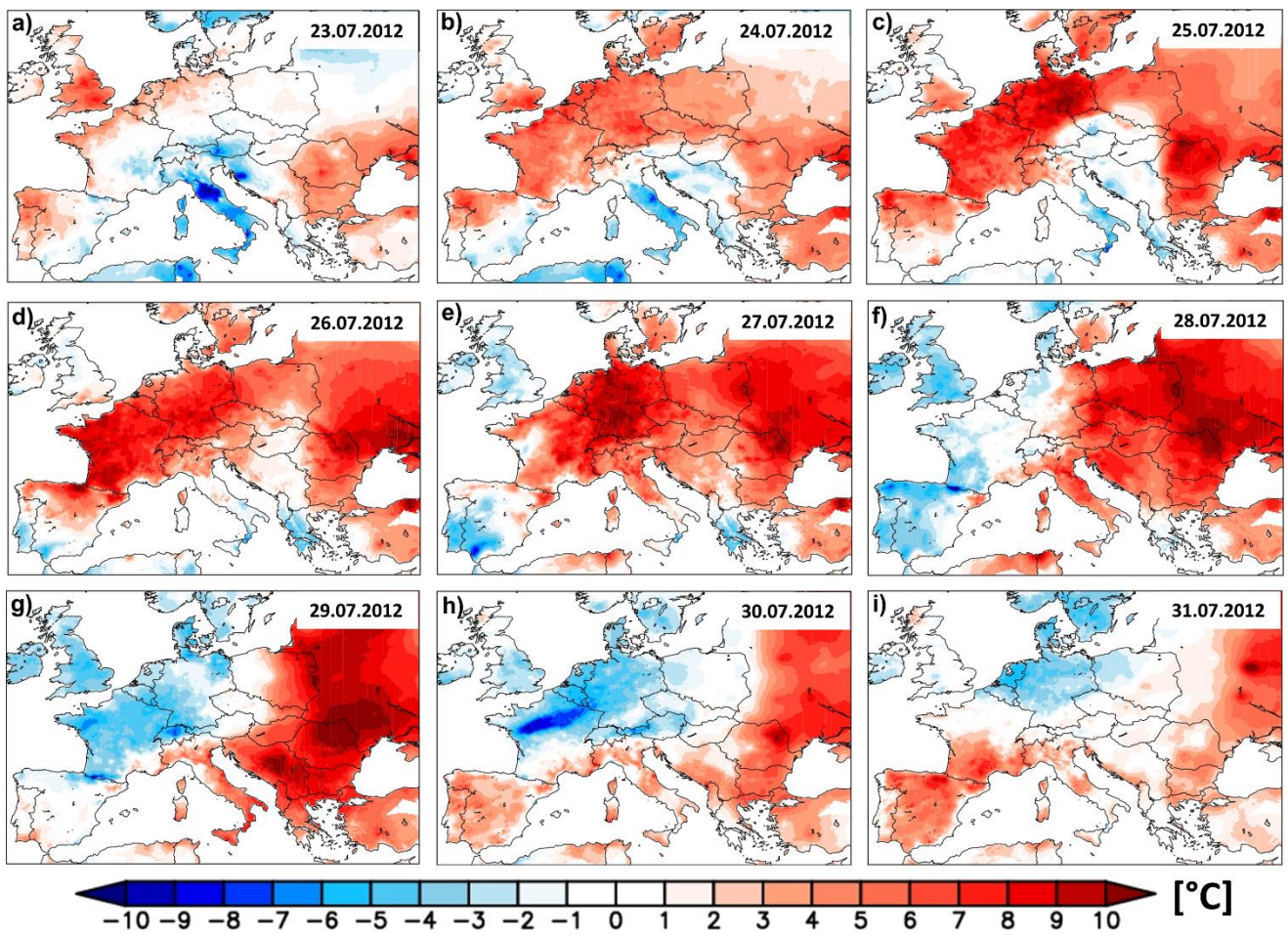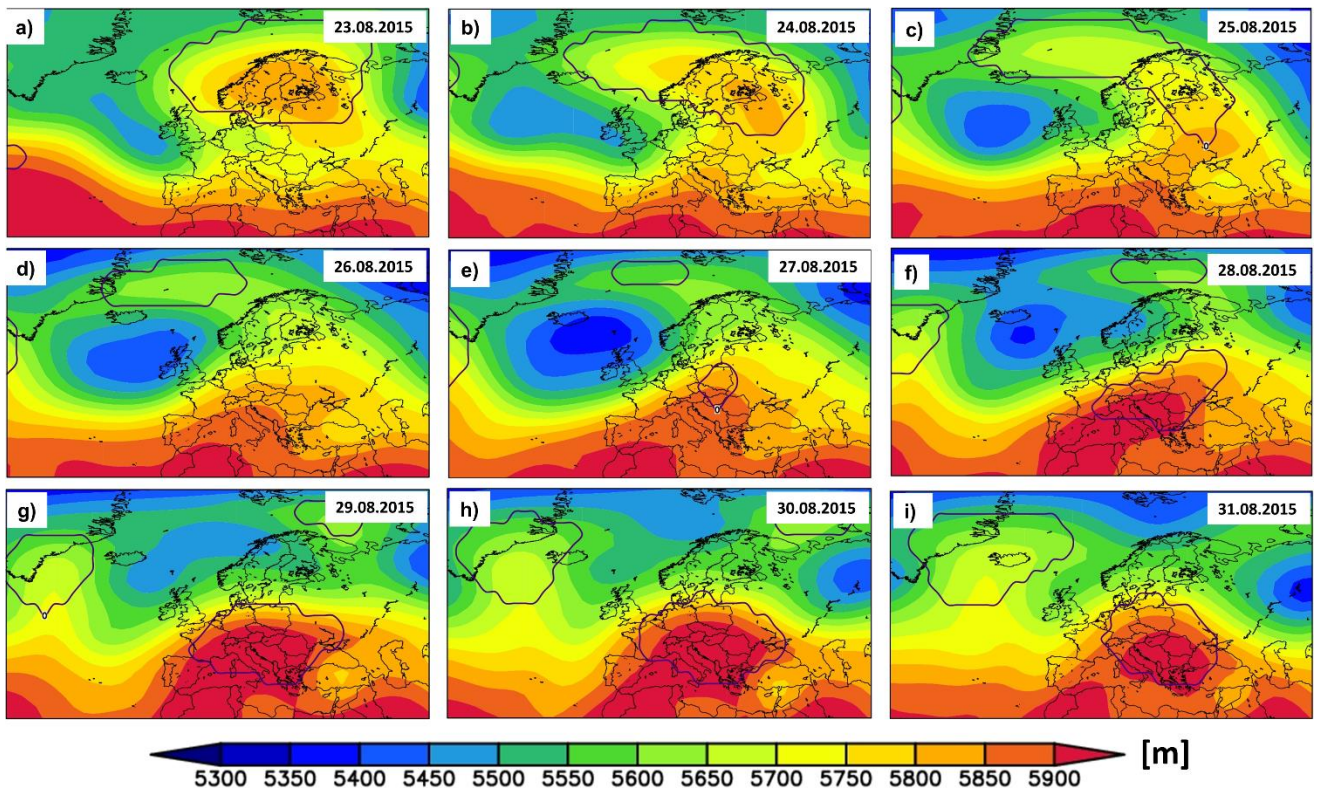
**Figure S5.** Evolution of the daily maximum temperature (Tx) anomaly over the period
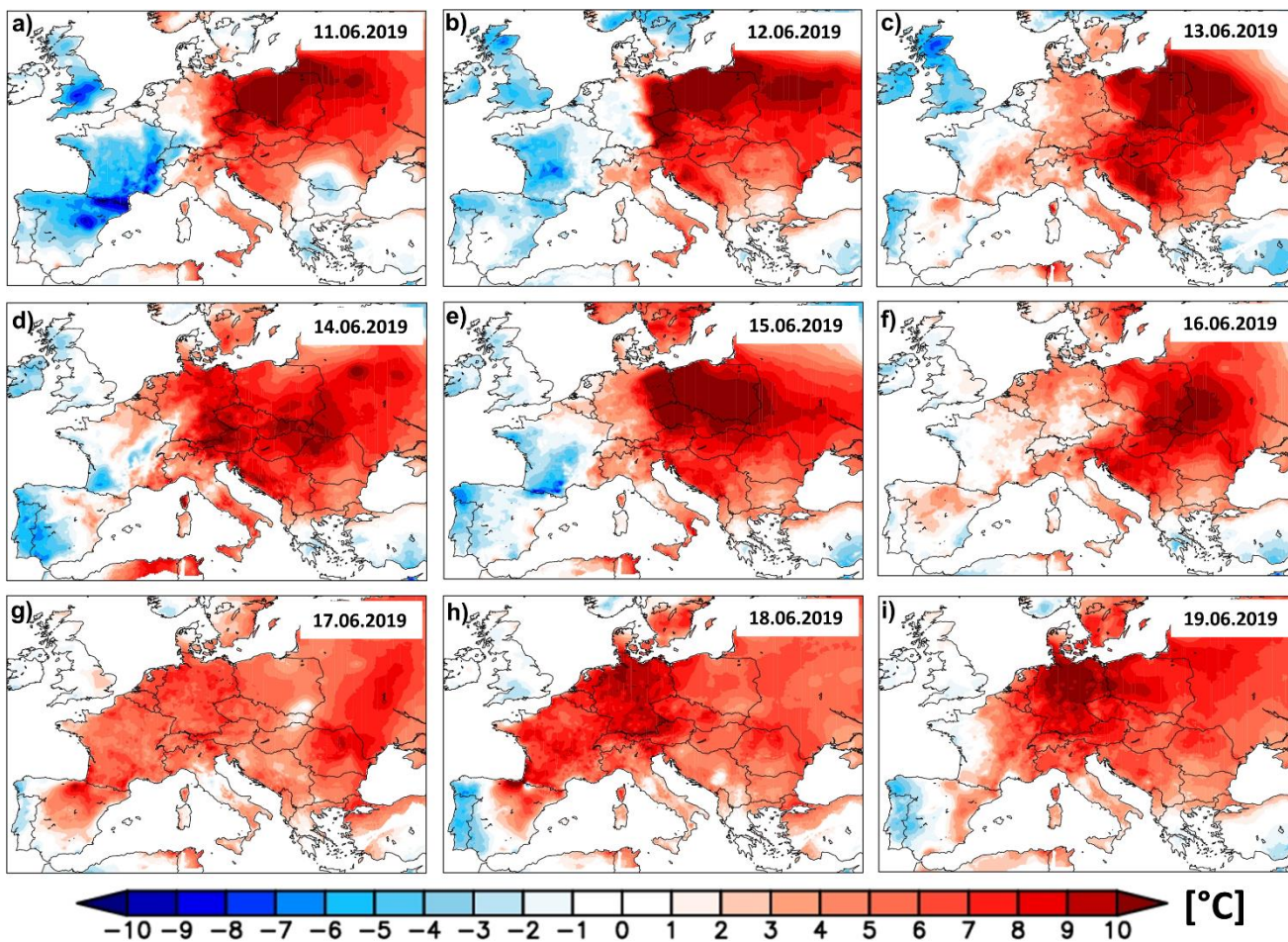23.07.2012 – 31.07.2012. The anomalies are computed relative to the base period 1971 – 2000.
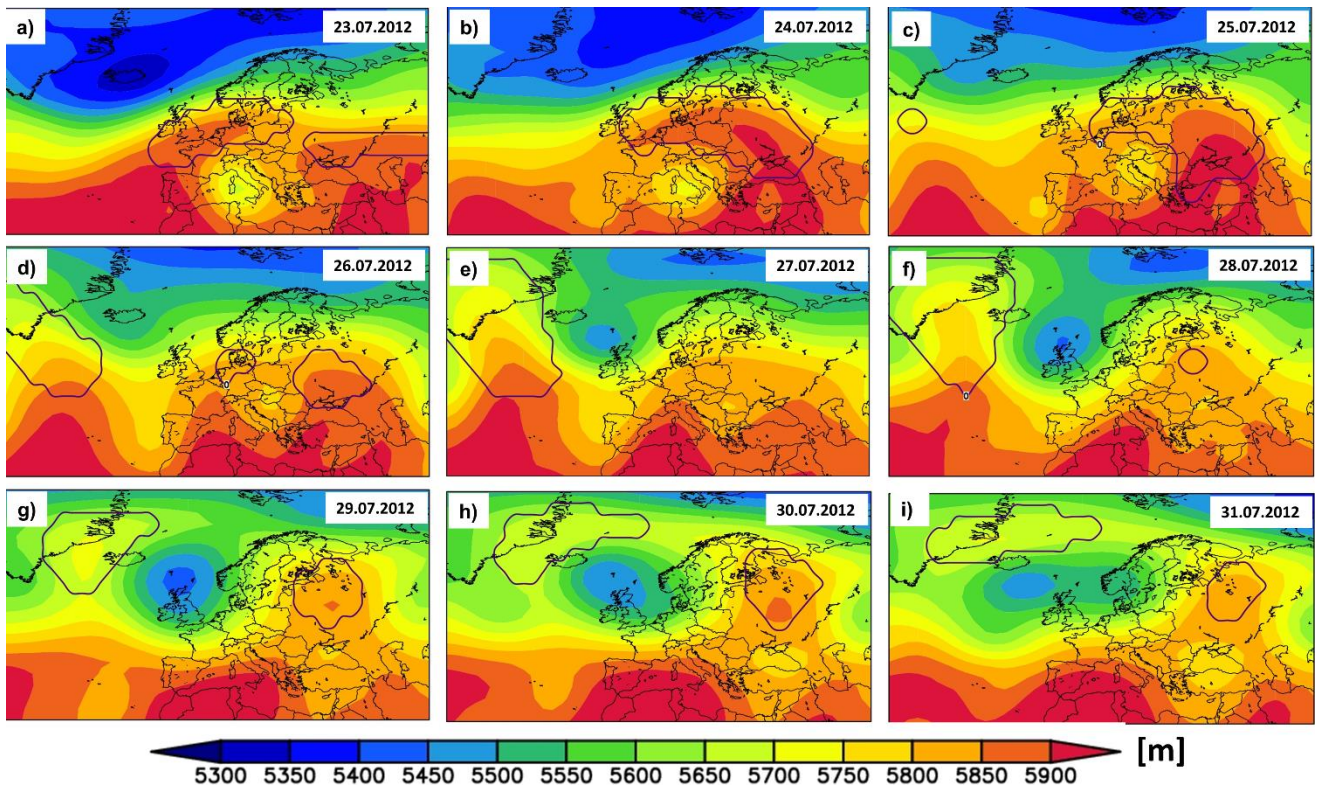
***Figure S6.*** Evolution of the daily geopotential height at 500mb (shaded colors) and the location of the 2D atmospheric blocking (contour lines)  over the period 23.07.2012 – 31.07.2012.
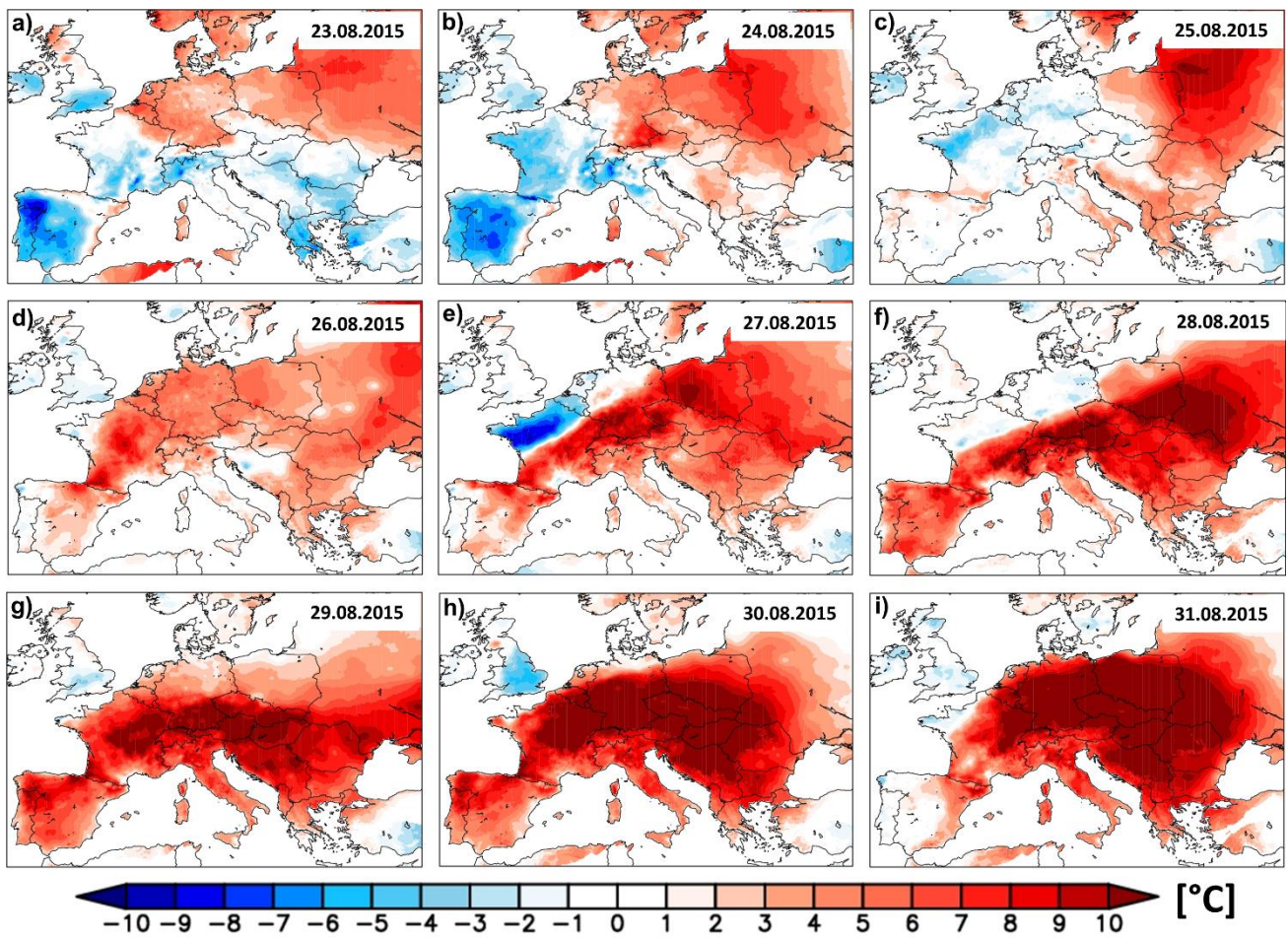
***Figure S7.*** Evolution of the daily maximum temperature (Tx) anomaly over the period
23.08.2015 – 31.08.2015. The anomalies are compute relative to the base period 1971 – 2000.

**Figure S8.** Evolution of the daily geopotential height at 500mb (shaded colors) and the location of the 2D atmospheric blocking (contour lines) over the period 23.078.2015 – 31.08.2015.

***Figure S9.*** Evolution of the daily maximum temperature (Tx) anomaly over the period
11.06.2019 – 19.06.2019. The anomalies are compute relative to the base period 1971 – 2000.
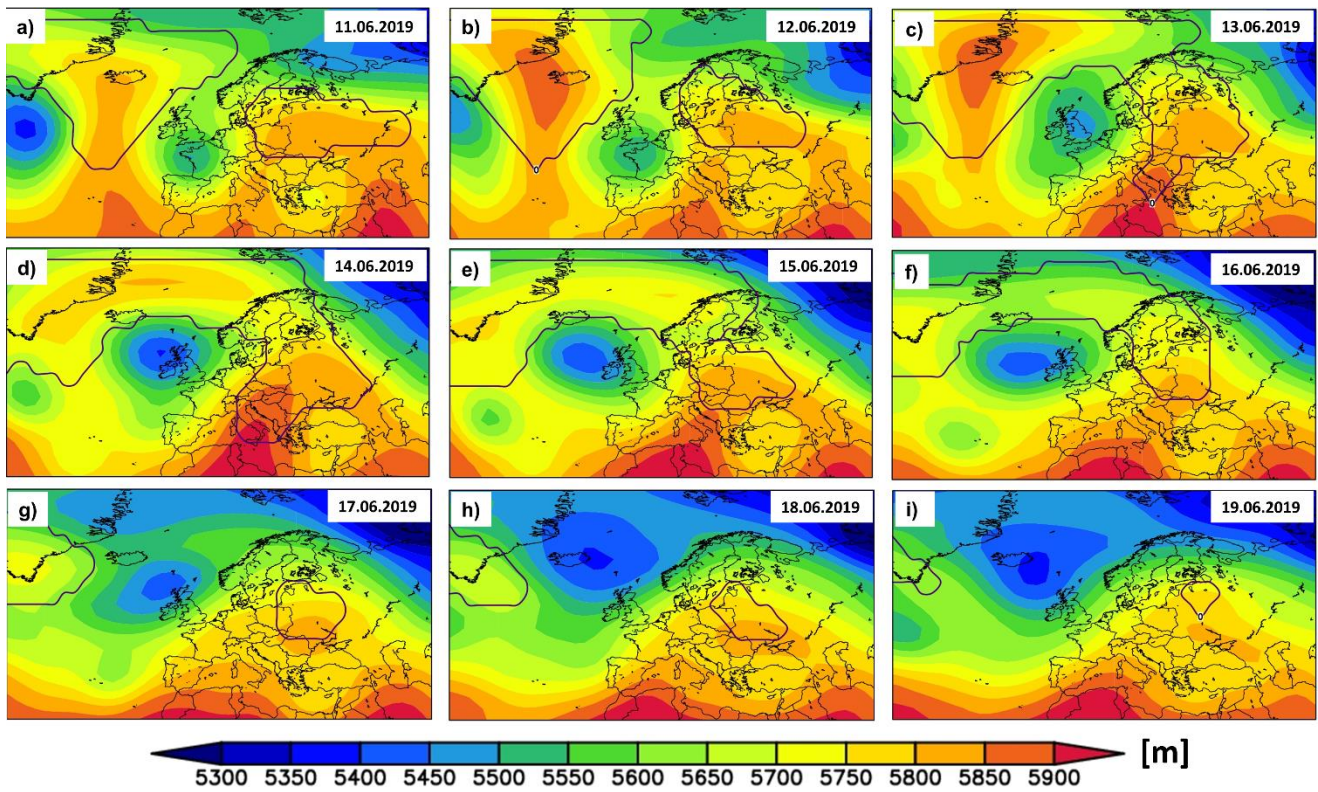
***Figure S10.*** Evolution of the daily geopotential height at 500mb (shaded colors) and the location of the 2D atmospheric blocking (contour lines) over the period 11.06.2019 – 19.06.2019.
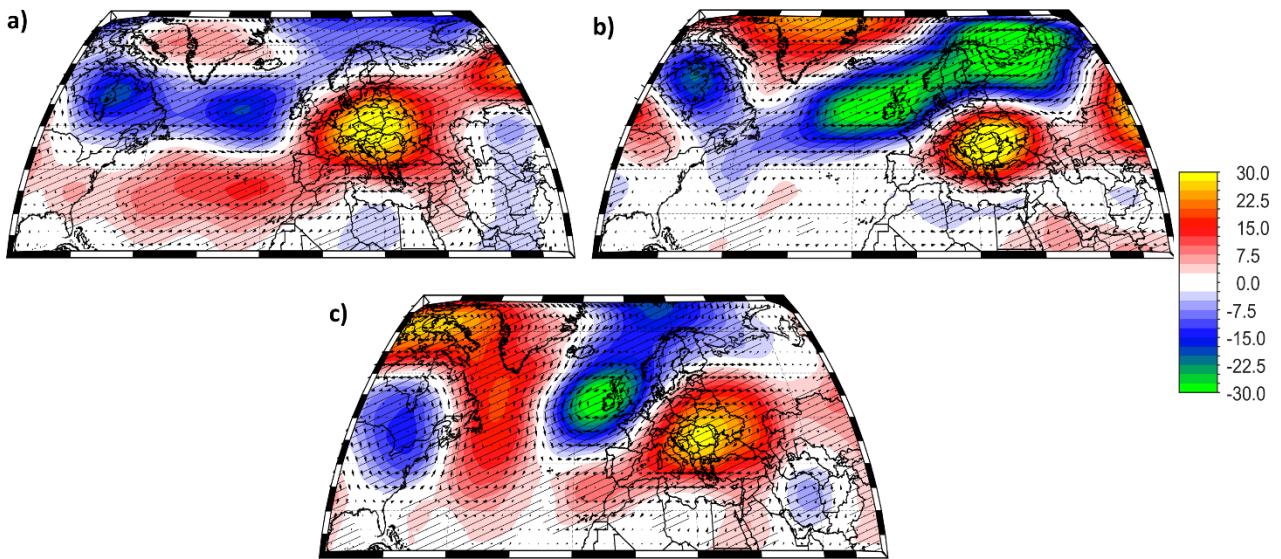
**Figure S11.** Large-scale atmospheric circulation patterns associated with the occurrence of monthly heat waves in the central part of Europe: a) The high composite map of June geopotential height at 500 mb (Z500) and the wind vectors at 500 mb corresponding to the cases when the area cover by a heat waves was higher than 20% of the country (June HW AREA> 20%); b) as in a) but for July and c) as in a) but for August. Units: Z500 [m].
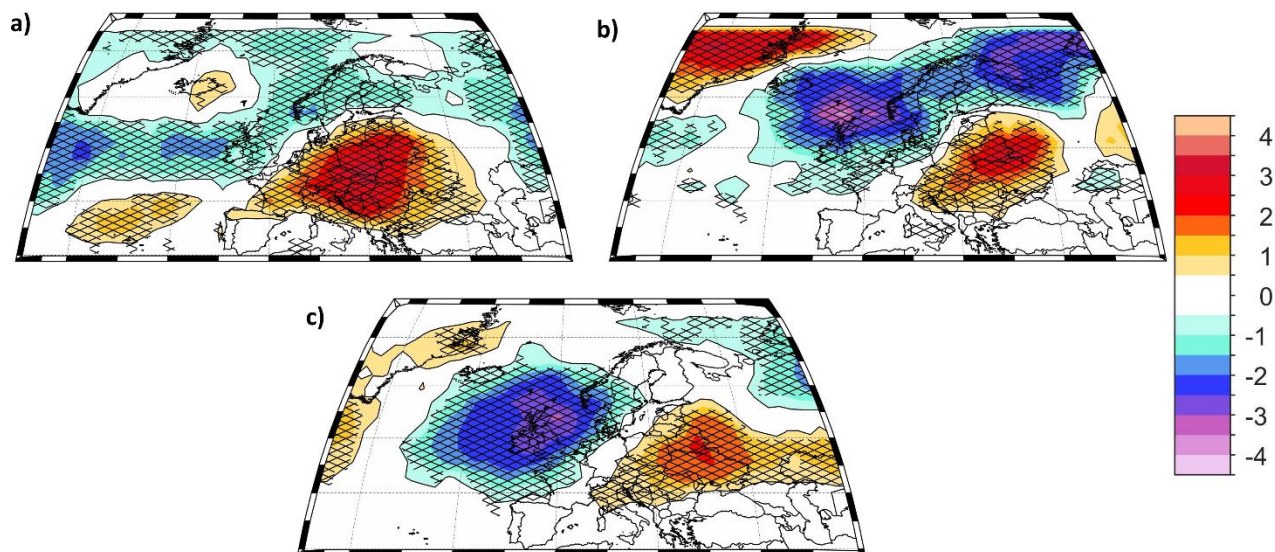
**Figure S12.** Frequency of the 2D atmospheric blocking associated with the occurrence of monthly heat waves in the central part of Europe: a) The high composite map of June 2D atmospheric blocking corresponding to the cases when the area cover by a heat waves was higher than 20% of the country (June HW AREA> 20%); b) as in a) but for July and c) as in a) but for August. Units: days/month.